

Article

Effects of Basicity and Al₂O₃ Content on Viscosity and Crystallization Behavior of Super-High-Alumina Slag

Shuai Wang , Ying Jiang, Yufeng Guo *, Zhuang Yang, Feng Chen , Lingzhi Yang and Guang Li

School of Minerals Processing and Bioengineering, Central South University, Changsha 410083, China; wang_shuai@csu.edu.cn (S.W.); jying007@csu.edu.cn (Y.J.); 205611068@csu.edu.cn (Z.Y.); csuchenf@csu.edu.cn (F.C.); yanglingzhi@csu.edu.cn (L.Y.); 215612109@csu.edu.cn (G.L.)

* Correspondence: yfguo@csu.edu.cn; Tel.: +86-0731-88830346

Abstract: The CaO-SiO₂-MgO-Al₂O₃ slags with high alumina content are widely applied in various pyrometallurgical processes. However, for super-high-alumina slags, especially for those with alumina content of more than 25 wt%, there is a lack of relevant studies about the properties of slag. The melting behavior, viscosity, structural property, and crystallization behavior of high-alumina slag with the fixed MgO content of 11.13 wt% and Al₂O₃ content from 27.61 wt% to 40 wt% were investigated. The results revealed that the liquidus temperatures and complete solidification temperatures of slag increased with the increasing binary basicity and Al₂O₃ content. The melting temperature and viscosity of the CaO-SiO₂-11.13wt%MgO-Al₂O₃ slag system increased with the increasing basicity from 0.8 to 1 and Al₂O₃ content from 27.61 wt% to 40 wt%. The increase in Al₂O₃ caused the formation of high-crystallinity and high melting point materials in the slag, such as spinel and Åkermanite. A large number of non-uniform phases could quickly crystallize out of the solids present in the slag melt, thereby increasing the slag viscosity and deteriorating the fluidity of the slag.

Keywords: viscosity; crystallization behavior; high-alumina slag; basicity; spinel



Citation: Wang, S.; Jiang, Y.; Guo, Y.; Yang, Z.; Chen, F.; Yang, L.; Li, G. Effects of Basicity and Al₂O₃ Content on Viscosity and Crystallization Behavior of Super-High-Alumina Slag. *Crystals* **2022**, *12*, 851. <https://doi.org/10.3390/cryst12060851>

Academic Editor: Carlos Rodriguez-Navarro

Received: 18 May 2022

Accepted: 14 June 2022

Published: 16 June 2022

Publisher's Note: MDPI stays neutral with regard to jurisdictional claims in published maps and institutional affiliations.



Copyright: © 2022 by the authors. Licensee MDPI, Basel, Switzerland. This article is an open access article distributed under the terms and conditions of the Creative Commons Attribution (CC BY) license (<https://creativecommons.org/licenses/by/4.0/>).

1. Introduction

Viscosity is a critical property of slag that affects the metallurgical process [1–7]. The CaO-SiO₂-MgO-Al₂O₃ slag system is well-known for its widespread use in pyrometallurgical operations [8–10]. The amount of high-quality iron resources decreases with the continuous exploitation in the world; thus, the low-quality iron ores with high Al₂O₃ become a choice. The high-alumina iron ore is also employed as the raw material in the ironmaking process [11–15]. Furthermore, the high-alumina slag is used to recover platinum group metals (PGMs) from alumina-based spent catalysts with metals collection methods [16–18]. Moreover, a tremendous amount of slag with high Al₂O₃ is produced during the ferronickel alloy and ferrochromium alloy production process [19–21]. As we know, the fluidity property of slag has a considerable influence on the smelting process and separation of metals from slag [22–26]. Therefore, it is vital to study the viscosity and crystallization behavior of high-alumina slag.

At present, the effects of basicity and Al₂O₃ on viscosity have been reported by some researchers. Chen et al. [27] studied the viscosity of SiO₂-MgO-FeO-Al₂O₃-MgO slag with the Al₂O₃ content from 4 wt% to 10 wt%, and the results revealed that Al₂O₃ was a network former and could polymerize the slag, increasing viscosity. Gao et al. [9] measured the viscosity of SiO₂-CaO-MgO-9wt% Al₂O₃ slag and pointed out that the complex network structure of the molten slag was disaggregated into simple network units as the basicity increased from 0.4 to 1.0. The viscosity experiments of CaO-SiO₂-MgO-Al₂O₃ slag [28] suggested the slag viscosity decreased with the increasing basicity from 0.5 to 0.9 and increased with the increase in alumina content from 5% to 20%. However, the effects of basicity and Al₂O₃ content on slag viscosity and crystallization behavior have not been sufficiently investigated for high-alumina slag with Al₂O₃ content above 25 %.

In this work, the effects of binary basicity and Al_2O_3 content on the melting behavior, viscosity, structural property, and crystallization behavior of the $\text{CaO-SiO}_2\text{-Al}_2\text{O}_3\text{-11.13wt\%MgO}$ system were investigated. The melting behavior and viscosity of slag with different binary basicity (0.8–1.1) and alumina (27.61–40 wt%) were measured. In a high Al_2O_3 and MgO slag system, it is easy to form a high melting point and high-crystallinity phases. Therefore, the viscosity behavior of slag is inseparable from the melting and crystallization behavior of slag. This work can deepen the realization of basicity and Al_2O_3 content on melting behavior, viscosity, and phase transformation of super-high Al_2O_3 (27.61–40 wt%) and high MgO (11.13 wt%) slag, and the interaction between these properties. In addition, this study can provide a technical basis for the efficient utilization of low-quality iron ores with high Al_2O_3 content.

2. Materials and Experimental Methods

2.1. Slag Sample Preparation

The slag samples in the experiment were half-synthetic slag based on a blast furnace slag from one steel company in China. The reagents used to modify the composition of slag include CaCO_3 (≥ 98 wt%), SiO_2 (≥ 99 wt%), MgO (≥ 98 wt%), and Al_2O_3 (≥ 99 wt%) reagents. The chemical composition of blast furnace slag is shown in Table 1. The chemical methods [29] were adopted for the chemical composition of blast furnace slag. The converted main compositions of the slag are 32.37 wt% SiO_2 , 27.61 wt% Al_2O_3 , 28.89 wt% CaO , 11.13 wt% MgO , and the binary basicity (CaO/SiO_2) is 0.89. The XRD pattern of the blast furnace slag is shown in Figure 1. As shown in Figure 1, the main phase of blast furnace slag is spinel (MgAl_2O_4). The half-synthetic slags were prepared by mixing the practical blast furnace slag and chemical reagents with a fixed mass ratio of 2:1. In this way, the chemical compositions of the slag sample are closer to the actual slag compositions. The designed chemical compositions of the half-synthetic slags are shown in Table 2. It could be seen that the CaO/SiO_2 ratio ranged from 0.8 to 1.1, and alumina ranged from 27.61 wt% to 40 wt%. All reagents except CaCO_3 powder were roasted at 1000 °C for one hour to remove carbonate and water. Appropriate amounts of the blast furnace slag powder and reagents were weighed and then mixed in an agate mortar to ensure composition uniformity. After that, one part of the mixtures was premelted in an electric furnace at 1500 °C for 1 h to attain the homogeneous samples. These pre-melted samples were used for subsequent viscosity measurement experiments. Additionally, another part of the mixtures were placed in a graphite crucible lined with molybdenum sheets and smelted in the electric furnace at 1500 °C for 1 h under the protection of N_2 gas (>99.9). Thereafter, the sample was removed from the furnace and quenched in cool water. After drying, the sample was crushed and ground for the melting properties tests.

Table 1. Chemical composition of blast furnace slag (mass fraction, %).

SiO_2	CaO	Al_2O_3	MgO	FeO	TFe	MnO	S	TiO_2	Cr_2O_3	MFe
27.9	24.90	23.8	9.59	1.63	1.40	1.36	0.97	0.58	0.57	0.13

Table 2. Design of composition of high-alumina slag (mass fraction, %).

No.	Slag Composition				Binary Basicity ($B = \text{CaO/SiO}_2$)
	CaO	SiO_2	MgO	Al_2O_3	
1#	27.23	34.03	11.13	27.61	0.8
2#	29.02	32.24	11.13	27.61	0.9
3#	30.63	30.63	11.13	27.61	1.0
4#	32.09	29.17	11.13	27.61	1.1
5#	25.52	28.35	11.13	35.00	0.9
6#	23.15	25.72	11.13	40.00	0.9
7#	25.60	23.27	11.13	40.00	1.1

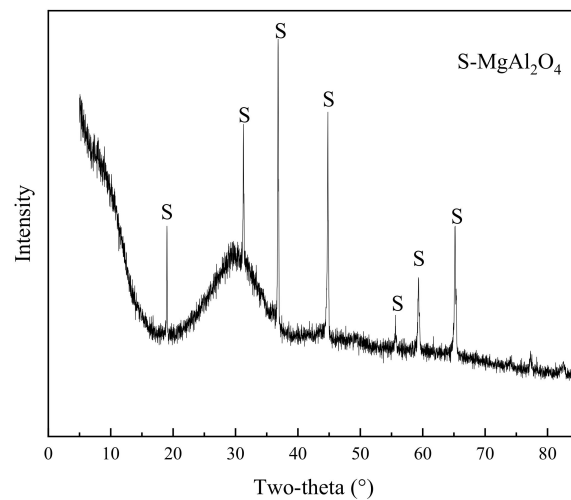


Figure 1. XRD pattern of blast furnace slag.

2.2. Experimental Methods

2.2.1. Viscosity Tests

The RTW-10 melt physical properties comprehensive testing instrument was applied to measure the viscosity value of the slag samples listed in Table 2. The schematic diagram of the experimental apparatus is illustrated in Figure 2, which consists of a high-temperature furnace, measuring system, gas purification system, and data acquisition system. The MoSi_2 heating element was used to heat the samples. The slag samples were placed into a molybdenum crucible surrounded by a graphite crucible, and a disassembled graphite sleeve was wrapped in the graphite crucible to hold the extra slag sample. The Mo spindle consisted of a bob and a shaft connected to a viscometer head. The viscometer was validated before the measurements adopting castor oil (A.R.) of known viscosity at room temperature.

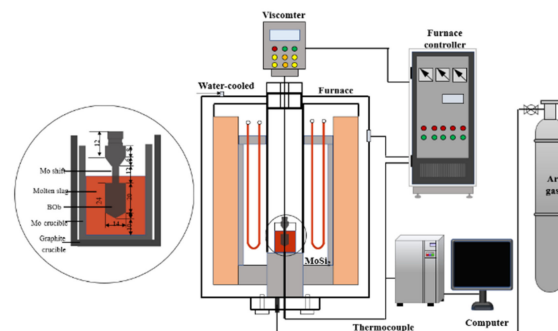


Figure 2. Schematic diagram of the slag viscosity measurement device.

During the experiment, about 125 g of premelted slag was added to the molybdenum crucible and then transferred to the furnace, and then it was set to heat at the rate of $5\text{ }^\circ\text{C min}^{-1}$ under the Ar atmosphere (>99.99%). The slag sample was premelted at $1550\text{ }^\circ\text{C}$ for 30 min to sustain the temperature and completely melt the slag sample. The rotating spindle was slowly immersed into the molten slag and rotated at a fixed rate of 200 r/min. The tip of the bob was positioned approximately 10 mm away from the bottom of the molybdenum crucible. The measurement was performed to cool down at a rate of $3\text{ }^\circ\text{C/min}$, and the target temperature was maintained for 0.5 h to ensure thermal equilibrium. The temperature and viscosity were recorded every 10 s by the data acquisition system. Furthermore, the final slag viscosity at each target temperature was the average of the measured value. When viscosity tests were over, the slag sample was reheated to $1500\text{ }^\circ\text{C}$ and then cooled to room temperature with the furnace to complete the slag crystallization.

As shown in Figure 5, the initial phase of the slag precipitation is spinel. The amount of spinel precipitation does not change significantly as the slag basicity increases from 0.8 to 1.1 with the fixed Al_2O_3 and MgO contents of 27.61 wt% and 11.13 wt%, respectively. Moreover, the precipitation silicate phase changes from $\text{CaAl}_2\text{Si}_2\text{O}_8$ to melilite ($\text{Ca}_2\text{MgSi}_2\text{O}_7$) when the basicity increases from 0.8 to 1.1. The amount of spinel phase increases as the Al_2O_3 content increases from 27.61 wt% to 40 wt% with the fixed slag basicity of 0.9. Furthermore, a small number of $\text{CaMg}_2\text{Al}_6\text{O}_{27}$ appear when the Al_2O_3 content of slag is up to 40 wt%. Moreover, as illustrated in Figure 5f,g, the $\text{CaAl}_2\text{Si}_2\text{O}_8$ disappears, and the $\text{Ca}_2\text{MgSi}_2\text{O}_7$ generates when the slag basicity increases from 0.9 to 1.1 at the fixed Al_2O_3 content of 40 wt%. Figure 5h shows the liquidus temperatures and complete solidification temperatures of slags with various basicity and Al_2O_3 contents. As shown in Figure 5h, both the liquidus temperature and complete solidification temperature of the slags increase with the basicity of slag increases from 0.8 to 1.1. In addition, the liquidus temperatures and complete solidification temperatures of the slags also increase with the increasing Al_2O_3 content, and this result is similar to the calculations of Ma et al. [31].

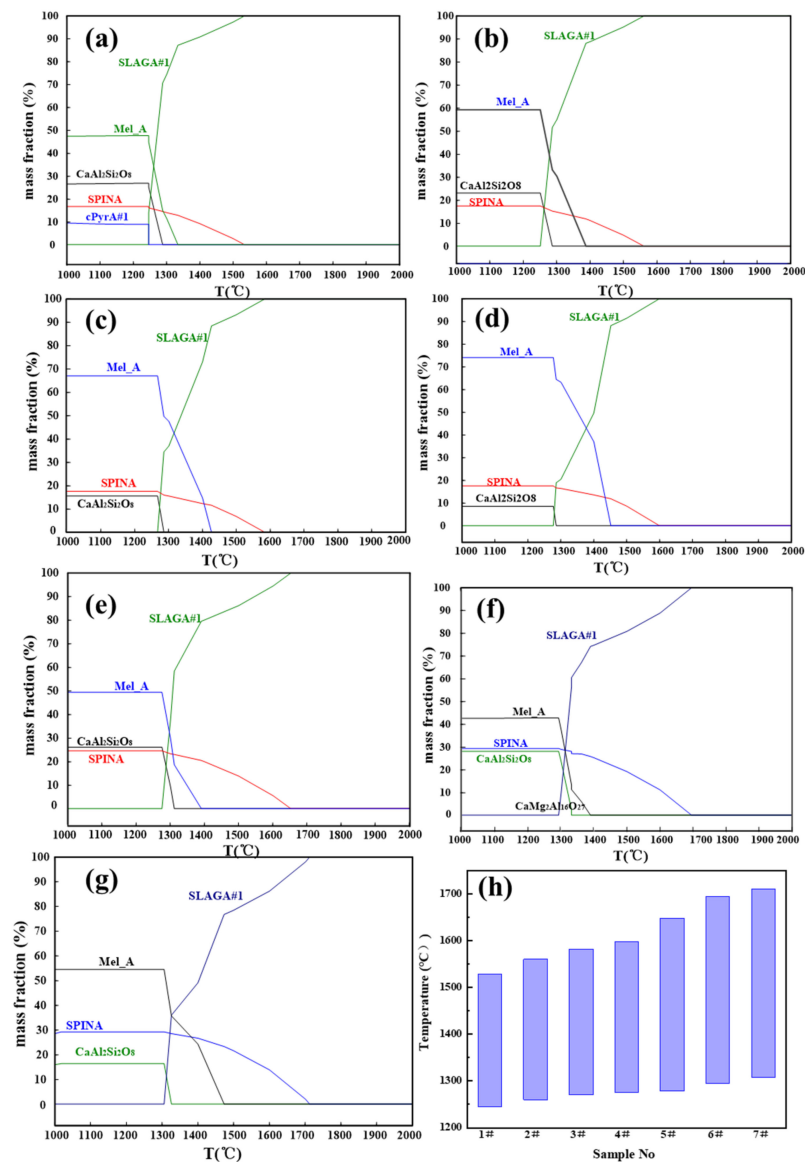


Figure 5. Equilibrium phase compositions of the high-alumina slags at various temperatures. (a) $B = 0.8$, (b) $B = 0.9$, (c) $B = 1.0$, (d) $B = 1.1$, (e) $B = 0.9$, $\text{Al}_2\text{O}_3 = 35$ wt%, (f) $B = 0.9$, $\text{Al}_2\text{O}_3 = 40$ wt%, (g) $B = 1.1$, $\text{Al}_2\text{O}_3 = 40$ wt%, and (h) the liquidus temperatures and complete solidification temperatures.

3.2. Melting Properties

Figure 6 shows the effects of the slag basicity on the melting temperatures of slags. It can be seen that the melting temperatures ranged from 1220 °C to 1340 °C, and the basicity had a significant influence on the melting temperature of the high-alumina slag. The spherical temperature, hemispherical temperature, and flowing temperature increase gradually with the increasing binary basicity. When the basicity increased from 0.8 to 1.1, the hemispherical temperature increased from 1228 °C to 1327 °C, and the flowing temperature increased from 1242 °C to 1338 °C.

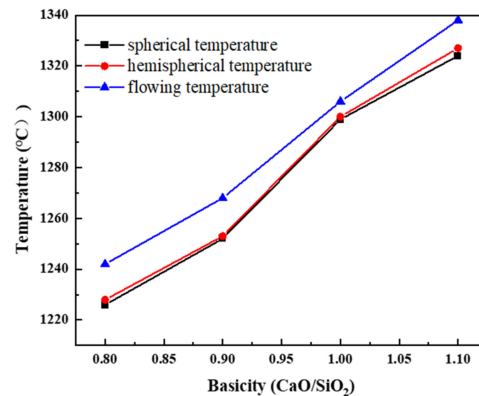


Figure 6. Effects of the slag basicity on the melting temperature of high-alumina slag ($\text{Al}_2\text{O}_3 = 27.61 \text{ wt}\%$; $\text{MgO} = 11.13 \text{ wt}\%$).

Figure 7 illustrates the influence of the Al_2O_3 content on the melting temperatures of the high-alumina slag. It indicates that the trends illustrated by the spherical temperature, hemispherical temperature, and flowing temperature with changing Al_2O_3 content were similar, and they significantly increased with increasing Al_2O_3 content. The hemispherical temperature of slag increases from 1253 °C to 1375 °C, and the flowing temperature increases from 1268 °C to 1402 °C as the Al_2O_3 content increases from 27.6 wt% to 40 wt%. The spherical temperature, hemispherical temperature, and flowing temperature reflect the melting properties of the slag, and high melting temperatures of slag may produce a solid phase during the smelting process, thus affecting the viscosity and fluidity of the slag. In our study, all characteristic temperatures increased with the increasing basicity from 0.8 to 1.1 and Al_2O_3 content from 27.6 wt% to 40 wt% in $\text{CaO-SiO}_2\text{-11.13 wt}\%\text{MgO-Al}_2\text{O}_3$ slag, which indirectly mirrored the possibility of the existence of the solid phase in the smelting process.

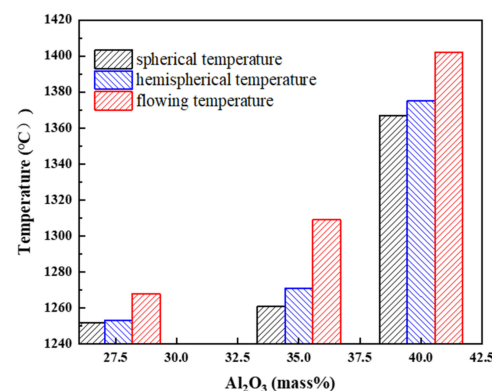


Figure 7. Effects of the Al_2O_3 content on the melting temperature of high-alumina slag. ($B = 0.9$, $\text{Al}_2\text{O}_3 = 27.61 \text{ wt}\%$).

3.3. Slag Viscosity

Figure 8 shows the viscosity-temperature curve of CaO-SiO₂-MgO-Al₂O₃ slag with basicity ranging from 0.8 to 1.1. It can be seen that the slag viscosity increases with the increasing basicity. As illustrated in Figure 9, the viscosity of the slags increases with the increasing Al₂O₃ content of slag. When the Al₂O₃ content of slag is fixed at 40 wt%, the measured slag viscosity is high and exceeds 5 Pa·s at 1522 °C. Figure 10 shows the effects of basicity on the viscosity of the slag system at 1500 °C and the effects of Al₂O₃ content on the viscosity of the slag system at 1520 °C, respectively. There is a linear relationship between viscosity and basicity of slag with fixed Al₂O₃ content of 27.61 wt% and MgO content of 11.13 wt% at 1500 °C, the viscosity of slag increased by approximately 0.14 Pa·s for every additional CaO/SiO₂ ratio of 0.1. The effect of Al₂O₃ content on the viscosity of slag is more significant.

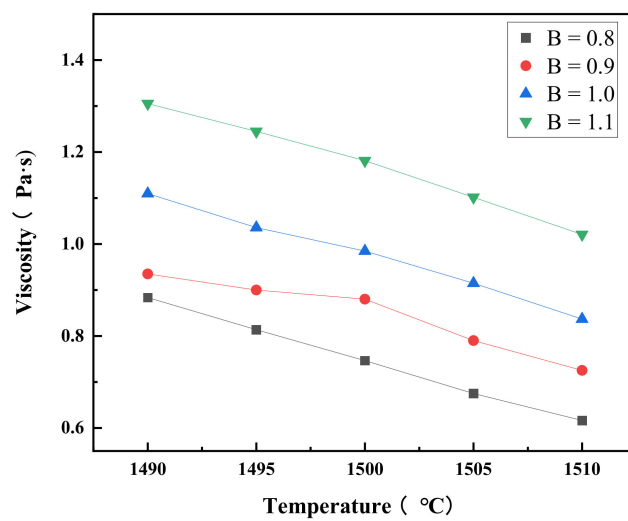


Figure 8. Effects of temperature on the viscosity of slag with different basicity (Al₂O₃ = 27.61 wt%; MgO = 11.13 wt%).

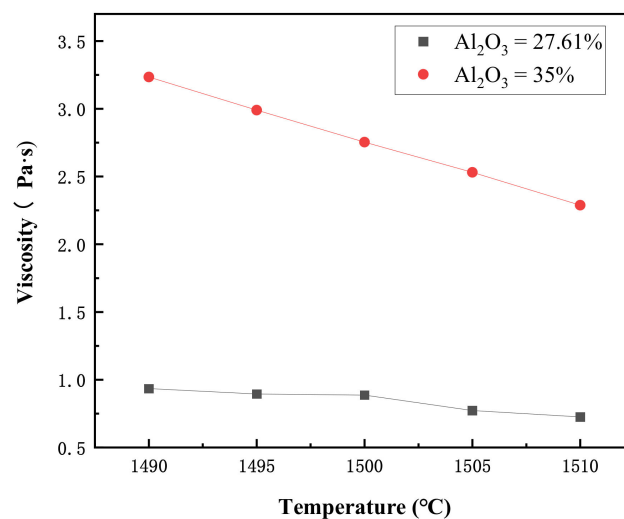


Figure 9. Effects of temperature on the viscosity of slag with different Al₂O₃ content (B = 0.9; MgO = 11.13 wt%).

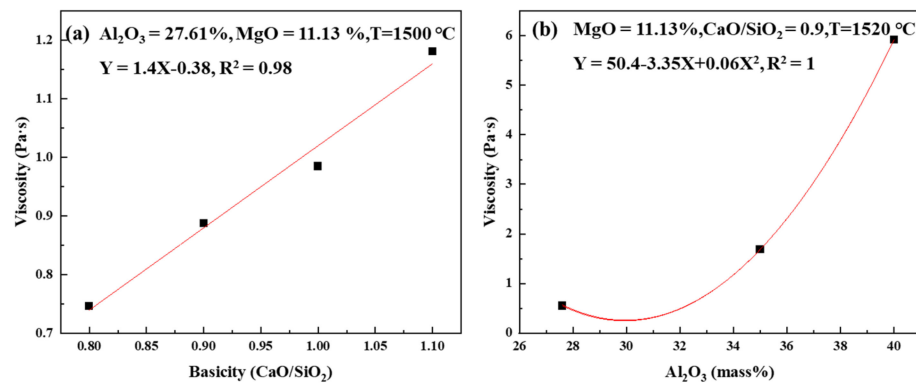


Figure 10. Effects of basicity (a) and Al₂O₃ content (b) on the viscosity of the CaO-SiO₂-MgO-Al₂O₃ slags.

Comparisons between the measured viscosities in the present study and other reports of the CaO-SiO₂-MgO-Al₂O₃ slags at 1500 °C are shown in Figure 11. From Figure 11a, it was noted that the slag viscosity increases with increasing basicity for the CaO-SiO₂-11.13wt%MgO-27.61wt%Al₂O₃ slags, a trend that is contrary to the results obtained by Hyuk Kim et al. [38] for CaO-SiO₂-10 wt%MgO-20 wt%Al₂O₃ slags and Y.M. Gao et al. [9] for CaO-SiO₂-13wt%MgO-9wt%Al₂O₃ slags. Moreover, it could be seen from Figure 11b that the viscosity of the slag increases with increasing Al₂O₃ content for the fixed MgO content of 11.13 wt% and basicity of 0.9. A similar observation was made by Lu Yao et al. [12] for the CaO-SiO₂-11wt%MgO-Al₂O₃ slag and Hyuk Kim et al. [38] for the CaO-SiO₂-10 wt%MgO-Al₂O₃ slag, but the viscosities were lower than that in this study.

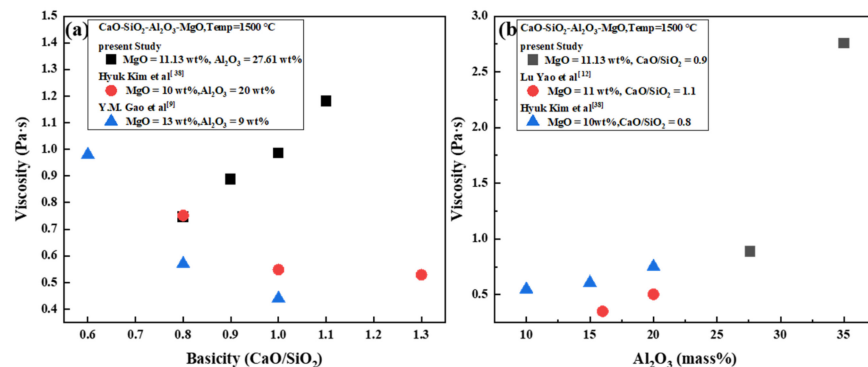


Figure 11. Comparisons of the effects of basicity (a) and Al₂O₃ content (b) on the viscosity of the CaO-SiO₂-MgO-Al₂O₃ slags at 1500 °C [9,12,38].

In addition, the structure of slags was determined by the FT-IR technique, and the results are shown in Figure 12. According to previous investigations [39–42], the FT-IR analysis of molten slag was typically situated in the wavenumber region between 1200 to 400 cm⁻¹. These regions at about 1200–800 cm⁻¹, 750–630 cm⁻¹, and 630–450 cm⁻¹, corresponding to [SiO₄]-tetrahedral stretching vibration bands, [AlO₄]-tetrahedral stretching vibration bands, and Si-O-Al bending, respectively. Furthermore, the [SiO₄]-tetrahedral stretching vibration bands can be classified depending on the values of NBO/Si, which corresponds to Q_{Si}⁰ (monomers, NBO/Si = 4), Q_{Si}¹ (dimers, NBO/Si = 3), Q_{Si}² (chains, NBO/Si = 2), and Q_{Si}³ (sheets, NBO/Si = 1), respectively. Figure 12a shows that the trough depth of [SiO₄]-tetrahedral band groups, [AlO₄]-tetrahedral band, and Si-O-Al bending were weakened when the CaO/SiO₂ ratio increased from 0.8 to 1. It indicated that the complicated network structures were disaggregated to simple structural units, which primarily attributed to the increase in free oxygen ions O²⁻. However, with the further increase

in the CaO/SiO₂ ratio from 1 to 1.1, the trough depth of [SiO₄]-tetrahedral band groups, [AlO₄]-tetrahedral band, and Si-O-Al bending became more remarkable, which signified that the silicate network became more complex because the compensation effects of Ca²⁺ on the [AlO₄] units are more pronounced when the CaO/SiO₂ ratio increases from 1 to 1.1. As shown in Figure 12b, both the trough depth of Q_{Si}⁰ and Q_{Si}¹ bands decreased while the trough depth of Q_{Si}² band increased with increasing Al₂O₃ content. The trough of [AlO₄]-tetrahedral stretching vibration bands had little change. This indicated that higher Al₂O₃ content tends to polymerize Si-O networks which play an active role in increasing viscosity [43,44].

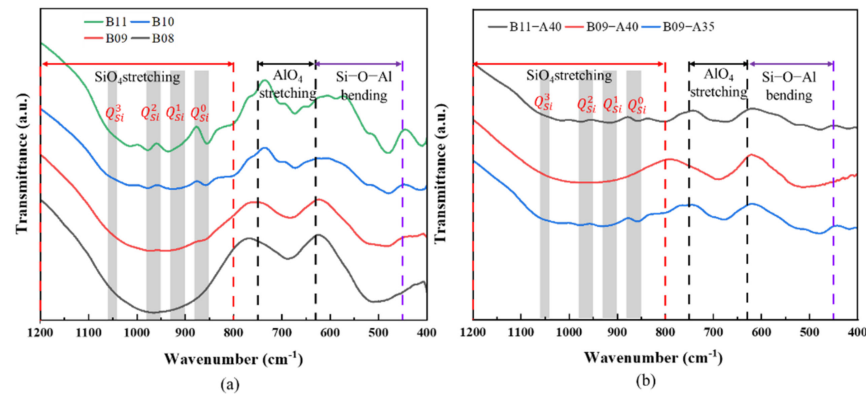


Figure 12. FT-IR transmittance spectra of CaO-SiO₂-MgO-Al₂O₃ slag with different basicity values.

As the Si-O network structures depolymerized with increasing Al₂O₃ content, the viscosity increased, which agreed with the current study. While the silicate network structures showed a tendency that depolymerized firstly and then polymerized with increasing CaO/SiO₂ from 0.8 to 1.1, the viscosity of slag increased consistently, which was a contradiction.

Moreover, the proportions of the slag liquid phase and solid phase were calculated by FactSage 8.0. As shown in Figure 13, the proportion of slag liquid phase decreased with increasing CaO/SiO₂ and Al₂O₃ content, and the proportion of solid phase increased at 1500 °C. Combining the phase diagram (Figure 4) and Figure 13 indicated that the slag samples exhibited a mixture of liquid and solid phases at 1500 °C, and the solid phase mainly consists of spinel.

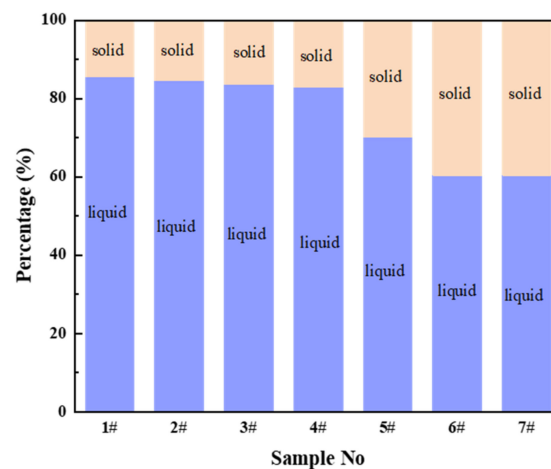


Figure 13. Variation of the main phases (liquid phase and solid phase) for high-alumina slag with different basicity and Al₂O₃ content at 1500 °C (FeO = 1.63%; MnO = 1.36%; TiO₂ = 0.58%; P(O₂) = 1.0 × 10⁻¹⁶ atm).

According to the above results, the inconsistency of viscosity changes that the viscosity of the slag increases with increasing basicity for the slags may be attributed to the high Al_2O_3 content and solid–liquid mixture behaviors. It is well known that partially molten materials or solid suspension liquids have a high viscosity value [27]. Additionally, the Roscoe model has been the most widely used to describe the viscosity of these melts [45,46]. The viscosity of the solid-containing melt is calculated by the following equation:

$$\eta = \eta_0(1 - af)^{-n} \quad (1)$$

where η and η_0 are the viscosity of solid-containing and solid-free melt, respectively; f is the concentration of solid particles; a and n are constants that are dependent on solid particles size.

As shown in Figures 11 and 13, increasing Al_2O_3 content increased both the viscosity of solid-containing and solid-free slag melt, indicating that Al_2O_3 acts as a network former in the slag system. However, increasing basicity decreased the viscosity of the slag system by providing additional free oxygen ions (O^{2-}) with Al_2O_3 content of slag was no more than 20 wt%. When the Al_2O_3 content of slag reached 27.61 wt%, slag samples exhibited a mixture of liquid and solid phases, resulting in high viscosity. It indicated that the effect of the solid phase on slag viscosity is predominant compared to the additional free oxygen and that effect is more pronounced at a higher Al_2O_3 .

3.4. Determination of Crystalline Phase

The phase compositions of slag with different Al_2O_3 content and basicity were investigated by XRD. It can be seen from Figure 14 that the main solid phases of $\text{CaO-SiO}_2\text{-MgO-Al}_2\text{O}_3$ slags are spinel (MgAl_2O_4) and Åkermanite ($\text{Ca}_2\text{MgSi}_2\text{O}_7$).

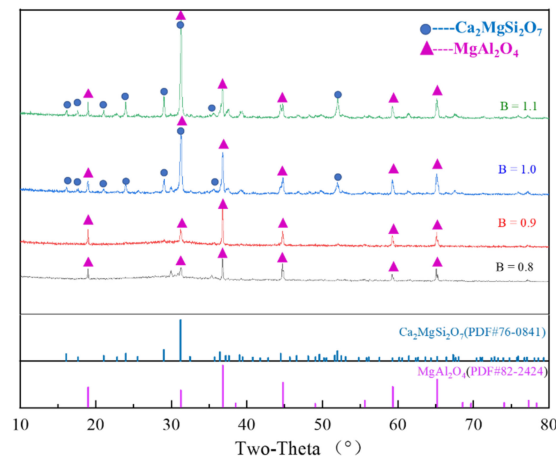


Figure 14. XRD patterns of the slowly cooled slag with different basicity (S-Spinel (MgAl_2O_4); A-Åkermanite ($\text{Ca}_2\text{MgSi}_2\text{O}_7$)).

The amount of spinel precipitation does not change significantly as the slag basicity increases from 0.8 to 1.1 with the fixed Al_2O_3 and MgO contents of 27.61 wt% and 11.13 wt%, respectively. When the basicity of slag is 0.8, the main phase is the spinel phase, and the diffraction peak of the Åkermanite phase is not obvious. There are significant diffraction peaks of the Åkermanite phase when the basicity of slag increases to 1.0. As the basicity continues to increase to 1.1, the Åkermanite phase increases further. The XRD patterns of slag with different Al_2O_3 content and the fixed binary basicity of 0.9 and MgO content of 11.13 wt% are illustrated in Figure 15. As shown in Figure 15, the main phase of slag is the spinel phase, which also increases with the increasing Al_2O_3 content. These regulations of crystalline phases are fit with the thermodynamic calculations.

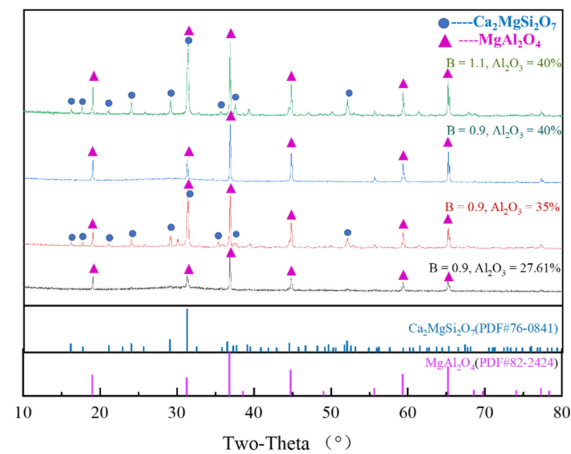


Figure 15. XRD patterns of the slowly cooled slag with different Al_2O_3 content and basicity (S-Spinel (MgAl_2O_4); A-Åkermanite ($\text{Ca}_2\text{MgSi}_2\text{O}_7$)).

The effects of basicity and Al_2O_3 content on the microstructure of high-alumina slag were observed, and the proportions of the solid phase in high-alumina slag were determined by Image J software and shown in Figure 16. As the basicity increased from 0.8 to 1.1, the size of solid particles became larger, and the proportion of solid phase in slag increased from 13.86% to 25.41%. This result agrees with the theoretical calculations in Figure 13 and also explains the increase in viscosity with increasing basicity. With higher Al_2O_3 content, a large number of fine solid phases emerged, and the percentage of crystals phase continues to increase, resulting in a more significant effect on viscosity.

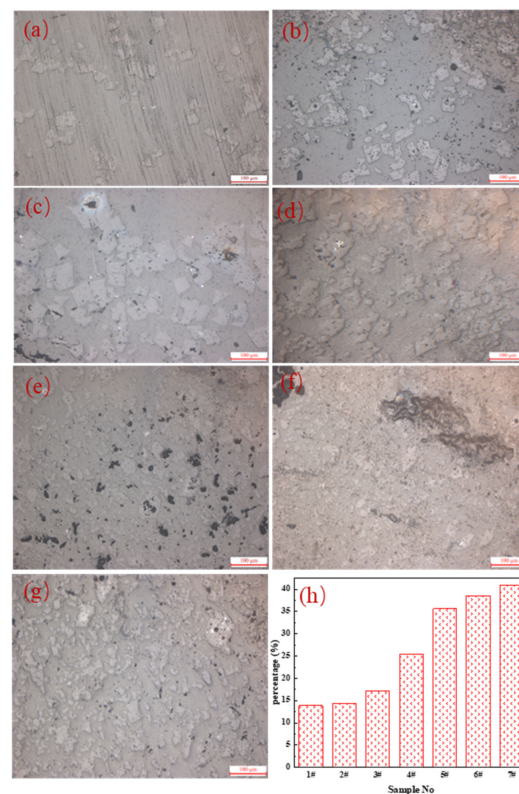


Figure 16. The effects of basicity and Al_2O_3 content on the microstructure of high-alumina slag. (a) $B = 0.8$, (b) $B = 0.9$, (c) $B = 1.0$, (d) $B = 1.1$, (e) $B = 0.9$, $\text{Al}_2\text{O}_3 = 35$ wt%, (f) $B = 0.9$, $\text{Al}_2\text{O}_3 = 40$ wt%, (g) $B = 1.1$, $\text{Al}_2\text{O}_3 = 40$ wt%, and (h) proportion of solid phase in high-alumina slag (determined by Image J software).

Briefly, the increases in basicity and Al_2O_3 content caused an ascendance in the melting temperature and viscosity of slags, which are detrimental to reducing energy consumption and metal–slag separation. In addition, The Al_2O_3 content has a strong influence on the structure of slag. As the Al_2O_3 content increased, the number of aluminum oxide tetrahedra $[\text{AlO}_4]^{5-}$ which formed by the absorption of O^{2-} by the Al_2O_3 increased, causing the formation of complex compounds with high crystallinity and high melting points, such as spinel. As the Al_2O_3 content increased further, Åkermanite and other mineral phase components that have a greater impact on the slag emerge, making the internal structure more complex and thus forming many non-uniform phases that can easily crystallize out of the solids present in the slag melt, causing the viscosity of the slag to become greater and the fluidity of the slag to become worse.

4. Conclusions

The effects of basicity and Al_2O_3 content on the melting behavior, viscosity, structural property, and crystallization behavior of super-high-alumina (27.61–40 wt%) slag were investigated. At a fixed MgO content of 11.13 wt% and Al_2O_3 content of 27.61 wt%, the melting temperature, viscosity, and crystals phase (spinel and Åkermanite) increased when the basicity increased from 0.8 to 1.1. The viscosity of slag increased by approximately 0.14 Pa·s for every additional CaO/SiO₂ ratio of 0.1 at 1500 °C. The proportion of crystal phase in slag increased from 13.86% to 25.41%. At a fixed MgO content of 11.13 wt% and basicity of 0.9 or 1.1, the melting temperature, viscosity, and crystal phase (spinel and Åkermanite) increased with the increasing Al_2O_3 content from 27.61–40 wt%. The Al_2O_3 content has a strong influence on the slag, When the Al_2O_3 content of slag is fixed at 40 wt%, the measured slag viscosity is high and exceeds 5 Pa·s at 1522 °C, and the proportion of solid phase in slag increased to more than 35%.

Author Contributions: Conceptualization, Y.G. and S.W.; methodology, S.W.; validation, F.C. and L.Y.; formal analysis, G.L.; writing—original draft preparation, S.W. and Y.J.; writing—review and editing, Y.G.; visualization, S.W.; supervision, Y.G. and S.W.; data curation, Z.Y. All authors have read and agreed to the published version of the manuscript.

Funding: This research was funded by the National Natural Science Foundation of China, grant number 52104345; the Major Science and Technology Special Project of Yunan Province, grant number 202002AB080001-1.

Institutional Review Board Statement: Not applicable.

Informed Consent Statement: Not applicable.

Data Availability Statement: Data sharing is not applicable to this article.

Acknowledgments: The authors would like to acknowledge the financial supports from the National Natural Science Foundation of China (52104345) and the Major Science and Technology Special Project of Yunan Province (202002AB080001-1).

Conflicts of Interest: The authors declare no conflict of interest.

References

1. Wu, T.; Wang, Q.; Yu, C.; He, S. Structural and viscosity properties of CaO-SiO₂-Al₂O₃-FeO slags based on molecular dynamic simulation. *J. Non-Cryst. Solids* **2016**, *450*, 23–31. [[CrossRef](#)]
2. Liu, Y.; Bai, C.; Lv, X.; Wei, R. Molecular dynamics simulation on the influence of Al₂O₃ on the slag structure at 1873 K. *Mater. Today Proc.* **2015**, *2*, 453–459. [[CrossRef](#)]
3. Sukenaga, S.; Saito, N.; Kawakami, K.; Nakashima, K. Viscosities of CaO-SiO₂-Al₂O₃-(R₂O or RO) melts. *ISIJ Int.* **2006**, *46*, 352–358. [[CrossRef](#)]
4. Zhan, W.; Liu, Y.; Shao, T.; Han, X.; Pang, Q.; Zhang, J.; He, Z. Evaluating the effect of MgO/Al₂O₃ ratio on thermal behaviors and structures of blast furnace slag with low carbon consumption. *Crystals* **2021**, *11*, 1386. [[CrossRef](#)]
5. Ghosh, D.; Krishnamurthy, V.A.; Sankaranarayanan, S.R. Application of optical basicity to viscosity of high alumina blast furnace slags. *J. Min. Metall.* **2010**, *46*, 41–49. [[CrossRef](#)]

6. Liu, W.; Xing, X.D.; Zuo, H.B. Effect of TiO₂ on viscosity and sulfide capacity of blast furnace slag containing barium. *ISIJ Int.* **2020**, *60*, 1886–1891. [[CrossRef](#)]
7. Marvila, M.T.; Azevedo, A.R.G.d.; Matos, P.R.d.; Monteiro, S.N.; Vieira, C.M.F. Rheological and the fresh state properties of alkali-activated mortars by blast furnace slag. *Materials* **2021**, *14*, 2069. [[CrossRef](#)]
8. Xiang, D.; Shen, F.; Jiang, X.; Gao, Q.; Zheng, H. Effect of unburned pulverized coal on the melting characteristics and fluidity of blast furnace slag. *Crystals* **2021**, *11*, 579. [[CrossRef](#)]
9. Gao, Y.M.; Wang, S.B.; Hong, C.; Ma, X.J.; Yang, F. Effects of basicity and MgO content on the viscosity of the SiO₂-CaO-MgO-9wt%Al₂O₃ slag system. *Int. J. Miner. Metall. Mater.* **2014**, *21*, 353–362. [[CrossRef](#)]
10. Kong, W.G.; Liu, J.H.; Yu, Y.W.; Hou, X.M.; He, Z.J. Effect of w(MgO)/w(Al₂O₃) ratio and basicity on microstructure and metallurgical properties of blast furnace slag. *Steel Res. Int.* **2021**, *10*, 1223–1232. [[CrossRef](#)]
11. Yan, Z.; Lv, X.; Zhang, J.; Qin, Y.; Bai, C. Influence of MgO, Al₂O₃ and CaO/SiO₂ on the viscosity of blast furnace type slag with high Al₂O₃ and 5 wt-% TiO₂. *Can. Metall. Q.* **2016**, *55*, 160215144748001. [[CrossRef](#)]
12. Yao, L.; Ren, S.; Wang, X.; Liu, Q.; Liu, J. Effect of Al₂O₃, MgO, and CaO/SiO₂ on viscosity of high alumina blast furnace slag. *Steel Res. Int.* **2016**, *87*, 241–249. [[CrossRef](#)]
13. Zhang, X.; Jiang, T.; Xue, X.; Hu, B. Influence of MgO/Al₂O₃ ratio on viscosity of blast furnace slag with high Al₂O₃ content. *Steel Res. Int.* **2016**, *87*, 87–94. [[CrossRef](#)]
14. Yan, Z.; Pang, Z.; Lv, X.W.; Qiu, G.; Bai, C. Physicochemical Properties of High Alumina Blast Furnace Slag. In *TMS Annual Meeting & Exhibition*; Springer: Cham, Switzerland, 2018; Volume 279-286, pp. 279–286. [[CrossRef](#)]
15. Dong, L.; Yan, Z.; Lv, X.; Jie, Z.; Bai, C.B. Transition of blast furnace slag from silicate-based to aluminate-based: Structure evolution by molecular dynamics simulation and raman spectroscopy. *Metall. Mater. Trans. B* **2016**, *48*, 1–9.
16. Zhao, J.; Cui, H.; Bao, S.; Tong, W.; Wu, Y.; Dong, H. Theoretical and experimental study on recovery of Platinum group metals by copper trapping method. *Chin. J. Nonferrous Met.* **2019**, *29*, 2820–2825.
17. Dong, H.; Zhao, J.; Chen, J.; Wu, Y.; Li, B. Recovery of platinum group metals from spent catalysts: A review. *Int. J. Mineral. Processing* **2015**, *145*, 108–113. [[CrossRef](#)]
18. Zheng, H.; Ding, Y.; Wen, Q.; Zhao, S.; He, X.; Zhang, S.; Dong, C. Slag design and iron capture mechanism for recovering low-grade Pt, Pd, and Rh from leaching residue of spent auto-exhaust catalysts. *Sci. Total Environ.* **2022**, *802*, 149830. [[CrossRef](#)]
19. Zhang, T.; Zhang, H.; Dai, S.; Huang, D.; Wang, W. Variation of viscosity and crystallization properties of synthetic ferronickel waste slag with Al₂O₃ content. *Ceram. Int.* **2021**, *47*, 22918–22923. [[CrossRef](#)]
20. Biswal, S.S.; Panda, C.; Sahoo, S.; Jena, T.; Panda, K.C. Assessment of factors influencing the elution of chromium from ferrochromium slag using factorial design of experiment. *Mater. Today Proc.* **2020**, *35*, 97–101. [[CrossRef](#)]
21. Ren, Y.; Ren, Q.; Wu, X.; Zheng, J.; Hai, O. Recycling of solid wastes ferrochromium slag for preparation of eco-friendly high-strength spinel–corundum ceramics. *Mater. Chem. Phys.* **2019**, *239*, 122060. [[CrossRef](#)]
22. Chenglin, Q.; Jianliang, Z.; Jiugang, S.; Weijia, L.; Zhixing, Z.; Xuesong, Z. Study of boronizing mechanism of high-alumina slag. *Steel Res. Int.* **2011**, *82*, 1319–1324. [[CrossRef](#)]
23. Shankar, A. Sulphur partition between hot metal and high alumina blast furnace slag. *Ironmak. Steelmak.* **2006**, *33*, 413–418. [[CrossRef](#)]
24. Khandelwal, D.; Sanapala, V. Measurement of Viscosity of High Alumina Blast Furnace Slags by Statistical Approach. Ph.D. Thesis, National Institute of Technology Rourkela, Odisha, India, 2015.
25. Sunahara, K.; Nakano, K.; Hoshi, M.; Inada, T.; Komatsu, S.; Yamamoto, T. Effect of high Al₂O₃ slag on the blast furnace operations. *Isij Int.* **2008**, *48*, 420–429. [[CrossRef](#)]
26. Sun, C.Y.; Liu, X.H.; Li, J.; Yin, X.T.; Song, S.; Wang, Q. Influence of Al₂O₃ and MgO on the Viscosity and Stability of CaO-MgO-SiO₂-Al₂O₃ Slags with CaO/SiO₂ = 1.0. *ISIJ Int.* **2017**, *57*, 978–982. [[CrossRef](#)]
27. Chen, Y.F.; Lv, X.M.; Pang, Z.D.; Lv, X.W. Effect of basicity and Al₂O₃ on viscosity of ferronickel smelting slag. *J. Iron Steel Res. Int.* **2020**, *27*, 1400–1406. [[CrossRef](#)]
28. Tang, X.L.; Zhang, Z.T.; Guo, M.; Zhang, M.; Wang, X.D. Viscosities Behavior of CaO-SiO₂-MgO-Al₂O₃ Slag With Low Mass Ratio of CaO to SiO₂ and Wide Range of Al₂O₃ Content. *J. Iron Steel Res. Int.* **2011**, *18*, 1–17. [[CrossRef](#)]
29. Zheng, G. Chemical analysis method standards and proficiency testing of laboratory for iron ore. *Metall. Anal.* **2015**, *35*, 37–44.
30. China Standardization Administration. *GB/T-219-2008*; Determination of Fusibility of Coal ash. China Standardization Administration: Beijing, China, 2008.
31. Ma, J.; Li, W.; Fu, G.; Zhu, M. Effect of Al₂O₃ on the viscosity and crystallization behavior of CaO-SiO₂-MgO-Al₂O₃-TiO₂-Cr₂O₃ slag. *JOM* **2021**, *74*, 159–166. [[CrossRef](#)]
32. Zhao, Y.; Zhang, Y.; Bao, S.; Chen, T.; Han, J. Calculation of mineral phase and liquid phase formation temperature during roasting of vanadium-bearing stone coal using FactSage software. *Int. J. Mineral. Process.* **2013**, *124*, 150–153. [[CrossRef](#)]
33. Bale, C.W.; Belisle, E.; Chartrand, P.; Deckerov, S.A.; Eriksson, G.; Gheribi, A.E.; Hack, K.; Jung, I.H.; Kang, Y.B.; Melancon, J.; et al. FactSage thermochemical software and databases, 2010–2016. *Calphad-Comput. Coupling Phase Diagr. Thermochem.* **2016**, *54*, 35–53. [[CrossRef](#)]
34. Wang, S.; Chen, M.; Guo, Y.F.; Jiang, T.; Zhao, B.J. Comparison of phase equilibria between FactSage predictions and experimental results in titanium oxide-containing system. *Calphad-Comput. Coupling Phase Diagr. Thermochem.* **2018**, *63*, 77–81. [[CrossRef](#)]

35. Rocha, V.C.d.; Silva, M.L.d.; Bielefeldt, W.V.; Vilela, A.C.F. Assessment of viscosity calculation for calcium-silicate based slags using computational thermodynamics. *REM Int. Eng. J.* **2018**, *71*, 243–252. [[CrossRef](#)]
36. Eriksson, G.; Konigsberger, E. FactSage and ChemApp: Two tools for the prediction of multiphase chemical equilibria in solutions. *Pure Appl. Chem.* **2008**, *80*, 1293–1302. [[CrossRef](#)]
37. Jung, I.-H.; Van Ende, M.-A. Computational thermodynamic calculations: FactSage from CALPHAD thermodynamic database to virtual process simulation. *Metall. Mater. Trans. B-Process. Metall. Mater. Process. Sci.* **2020**, *51*, 1851–1874. [[CrossRef](#)]
38. Kim, H.; Matsuura, H. Effect of Al₂O₃ and CaO/SiO₂ on the viscosity of calcium-silicate-based slags containing 10 mass pct MgO. *Metall. Mater. Trans. B* **2013**, *44*, 5–12. [[CrossRef](#)]
39. Kim, Y.; Min, D.-J. Viscosity and structural investigation of high-concentration Al₂O₃ and MgO slag system for FeO reduction in electric arc furnace processing. *Metals* **2021**, *11*, 1169. [[CrossRef](#)]
40. Shen, X.; Chen, M.; Wang, N.; Wang, D. Viscosity property and melt structure of CaO-MgO-SiO₂-Al₂O₃-FeO slag system. *ISIJ Int.* **2019**, *59*, 9–15. [[CrossRef](#)]
41. Huang, W.-J.; Zhao, Y.-H.; Yu, S.; Zhang, L.-X.; Ye, Z.-C.; Wang, N.; Chen, M. Viscosity property and structure analysis of FeO-SiO₂-V₂O₃-TiO₂-Cr₂O₃ Slags. *ISIJ Int.* **2016**, *56*, 594–601. [[CrossRef](#)]
42. Deng, L.; Zhang, X.; Zhang, M.; Jia, X. Effect of CaF₂ on viscosity, structure and properties of CaO-Al₂O₃-MgO-SiO₂ slag glass ceramics. *J. Non-Cryst. Solids* **2018**, *500*, 310–316. [[CrossRef](#)]
43. Li, T.; Sun, C.; Song, S.; Wang, Q. Influences of Al₂O₃ and TiO₂ content on viscosity and structure of CaO-8%MgO-Al₂O₃-SiO₂-TiO₂-5%FeO blast furnace primary slag. *Metals* **2019**, *9*, 743. [[CrossRef](#)]
44. Xu, C.-Y.; Wang, C.; Xu, R.-Z.; Zhang, J.-L.; Jiao, K.-X. Effect of Al₂O₃ on the viscosity of CaO-SiO₂-Al₂O₃-MgO-Cr₂O₃ slags. *Int. J. Miner. Metall. Mater.* **2021**, *28*, 797–803. [[CrossRef](#)]
45. Roscoe, R. The viscosity of suspensions of rigid spheres. *Br. J. Appl. Phys* **1952**, *3*, 267. [[CrossRef](#)]
46. Zhang, G.H.; Zheng, Y.L.; Chou, K.C. Influence of TiC on the Viscosity of CaO-MgO-Al₂O₃-SiO₂-TiC Suspension System. *ISIJ Int.* **2015**, *55*, 922–927. [[CrossRef](#)]